

Synthesis and stability of biomolecules under Earth’s upper mantle conditions

Tao Li,¹ Nore Stolte,¹ and Ding Pan^{1,2,3,*}

¹*Department of Physics, Hong Kong University of Science and Technology, Hong Kong, China*

²*Department of Chemistry, Hong Kong University of Science and Technology, Hong Kong, China*

³*HKUST Shenzhen-Hong Kong Collaborative Innovation Research Institute, Shenzhen, China*

(Dated: May 9, 2024)

Abstract

How life started on Earth is a long-time unsolved mystery. There are various hypotheses ranging from outer space to seabed. Here, we applied extensive ab initio molecular dynamics (AIMD) simulations to study chemical reactions of NH₃, H₂O, H₂, and CO at pressures (P) and temperatures (T) approximating the conditions of Earth’s upper mantle (*i.e.* 10 - 13 GPa, 1000 - 1400 K). Contrary to the previous assumption that larger organic molecules might readily dissociate in aqueous solutions at extreme P-T conditions, we found that many organic compounds formed and persisted in C-H-O-N fluids under these extreme conditions, including glycine, ribose, and uracil-like molecules. Particularly, our free energy calculations showed that the C-N bond is thermodynamically stable at 10 GPa and 1400 K. Moreover, our findings support the “RNA world” hypothesis, as we observed the exclusive formation of the 5-membered-ring form of ribose. By exploring the depths of Earth’s interior, we have uncovered a previously unexplored pathway through which life may have originated. These findings have contributed to our evolving understanding of the fundamental conditions necessary for life to arise on our planet.

INTRODUCTION

The origin of life on Earth remains a profound scientific mystery. Numerous hypotheses have been put forward, but none have been conclusively verified [1]. As early as ~ 150 years ago, Darwin proposed a “warm little pond” idea [2], which was later developed by Oparin and Haldane into the influential “primordial soup” theory in the 1920s [3], that is, the reactions of small molecules, such as CH_4 , NH_3 , H_2O , and CO_2 , leads to the abiotic origin of life on early Earth. In 1953, the famous Miller-Urey experiment was conducted to test this hypothesis at the presence of electric discharge [4]. Inspired by the “primordial soup” theory, various prebiotic conditions have been proposed for the origin of life, ranging from the interstellar medium (ISM) [5] or other planets [6, 7] to deep-sea hydrothermal vents [8].

Hydrothermal vents are fissures in Earth’s oceanic crust where hot water rich in gases and minerals is released. Those deep sea vents are considered to have suitable conditions for origin of life. The pressure (P) of hydrothermal vents is tens of MPa depending on the depth of water, and the temperature (T) can reach 700 K. It is widely believed that the origin of life is unlikely to occur in the deeper regions of the Earth, such as the upper mantle, where the pressure can reach up to ~ 13 GPa, accompanied by temperatures of ~ 1700 K; the extremely high P-T conditions could readily degrade crucial biomolecules in aqueous solutions [9]. Otake et al. studied the stability of amino acids and their oligomerization at 10–5.0 GPa and 453–673 K, and found that high pressure inhibited the decomposition of amino acids ; however, their experiments were conducted at the water-poor condition [10]. Previously, the fluids in Earth’s mantle were commonly modelled as simple mixtures of small volatile molecules, including H_2O , CO_2 , CO , CH_4 , and H_2 [11]. However, recent experimental and theoretical studies have revealed the significant roles played by chemical speciation, aqueous ions, and complexes in the supercritical geofluids within Earth’s lithosphere [12–16]. These findings have challenged the previous assumptions and shed light on the potential existence of larger organic molecules.

It is very challenging to study the origin of life in laboratory settings due to the extreme environments involved. Atomistic simulations based on first principles have been applied to study prebiotic chemistry, offering significant molecular insights [1]. Saitta *et al.* applied ab initio molecule dynamics (AIMD) and metadynamics simulations to study the Miller-Urey experiment, and found unexpected reaction intermediates including formic acid and formamide [17]. Goldman *et al.* applied AIMD simulations to investigate the formation of prebiotic compounds from impact-induced shock compression of cometary ices followed by expansion to ambient conditions, and found that the impact of cometary ices could produce amino acids independently of atmospheric conditions and Earth minerals [18–20]. AIMD simulations coupled with enhanced sampling techniques have also been applied to study the role of mineral surfaces in prebiotic chemistry [21–23]. Despite the numerous previous studies, the exploration of prebiotic chemistry within Earth’s upper mantle remains an uncharted territory.

Here, we applied extensive AIMD simulations to study the C-H-O-N fluids at 10–13 GPa and 1000–1400 K, the P-T conditions as found at the bottom of Earth’s upper mantle. We discovered a large range of organic molecules directly formed without any catalysts at extreme P-T conditions, including glycine, ribose, and uracil-like molecules. Our free energy calculation suggested that the C-N bond is thermodynamically stable at 10 GPa and 1400 K. Our study has provided valuable insights into a new potential avenue for the origin of life within Earth’s interior, expanding our understanding of the conditions necessary for life to emerge.

RESULTS AND DISCUSSION

We initially mixed the H_2O , H_2 , CO , and NH_3 molecules in the simulation box. The molecular number of each molecule is 15. We conducted AIMD simulations at three P-T conditions: 10 GPa and 1000 K, 10 GPa and 1400 K, and 13 GPa and 1400 K to see how chemical products vary with P and T. Those P-T conditions are typically found at the bottom of Earth’s upper mantle. After 400 ps simulations at each P-T condition, we found about 100 different organic species. Here we mainly focus on the formation of bio-relevant molecules, so we classify the organic molecules into six categories: “CN”, “ C_2N ”, “ CN_2 ”, “ C_2N_2 ”, “ C_3N_x ”, and “ C_4N_x ”, based on the numbers of carbon and nitrogen atoms, as shown in Table I. Fig. 1 shows the chemical structures of the representative species. Species with more than five carbon atoms are excluded due to their high instability and extremely short lifetime, typically lasting for only a few femtoseconds. The number and percentage of these CN-containing species as functions of time under three different P-T conditions are shown in Figures S5 and S6, respectively, which suggest that the concentrations of these species gradually stabilize over time.

At 10 GPa and 1000 K, most of the organic products belong to three main categories, as shown in Fig. 2(a). The “ C_2N_2 ” species account for more than half of the CN-containing species, followed by the “CN” species, and finally “ C_2N ”. Formamide is the primary product in the “CN” species [24]. It contains the peptide bond, which is a significant precursor for the production of more complex biomolecules, such as amino acids [25], nucleic acids, proteins, and even sugars [26, 27]. The “ C_2N ” species has the same CN-backbone (“-N-C-C-”) as that of glycine, suggesting that the “ C_2N ” species may be a potential reactant for the formation of amino acids. At this P-T condition, some of the “ C_2N ” species are not stable and can be transformed into the “ C_2N_2 ” species by reacting with ammonia or ammonium ions, so the CN-backbone of “ C_2N_2 ” is “-N-C-C-N-”, and one interesting molecule was identified as alpha-hydroxy-glycineamide (α -HGA).

With increasing the temperature to 1400 K along the isobar at 10 GPa, all the six categories of organic products at this P-T condition are observed. The “CN₂” and “C₄N_x” fractions are very small, while the other four species have similar fractions. Compared with 10 GPa and 1000 K, the portion of “C₂N₂” becomes smaller, while there are more “C₂N” species. The “C₂N” species formed here also share the same CN backbone (“-N-C-C-”) with glycine. Notably, in the “C₂N” species, it is possible to form α -hydroxyglycine, which can subsequently evolve into glycine through simple chemical reactions [17]. The “C₂N₂” species have the CN-backbone of“-N-C-C-N-”, including α -HGA and oxamide. They are important organic molecules in the formation of the building blocks of peptides [28]. Among the “CN” species, formamide remains the most abundant one. Additionally, the “CN₂” species with the “-N-C-N-” backbone was observed, which did not typically form at 10 GPa and 1000 K. One representative product of this species is methanediamine (CH₆N₂) [29], which was reported as a vital intermediate or precursor in the abiotic formation of nucleobases [30].

With increasing the pressure to 13 GPa at 1400 K, the “CN” species becomes dominating, and the “C₂N₂” species comes next. For the “CN” species, in addition to formamide, some other crucial precursors for producing more complex biomolecules are identified, such as carbamic acid [31], isocyanic acid [32], and formimidic acid [33]. The “C₂N₂” species exhibit a distinct CN-backbone compared to the two systems at 10 GPa, forming as “-C-N-C-N-”, which is present in the organic matter of allophanic acid. This kind of acid plays a vital role in the synthesis of biomolecules (*e.g.* uracil), and would be used in subsequent simulations. Surprisingly, the fraction of “C₂N” species sharply decreases to a small value, adopting a new CN-backbone structure of “-C-N-C-”, as observed in N-formylformamide [34]. This structural change makes it challenging for “C₂N” species formed here to evolve into glycine-like molecules or larger amino acids. In the “CN₂” species, we have discovered the presence of urea molecules. Urea is closely related with biological processes, so it would also serve as a valuable reactant for investigating the reactions to larger biomolecules.

For all the three P-T conditions, a common feature is that the “CN” and “C₂N₂” species

are always the major compositions among the six CN-containing species. Fig. 2 (b) shows the lifetime of these CN-containing species. The lifetime distribution in Fig. 2 (b) shows that the “CN” and “C₂N₂” species could exist for a longer time at all the three P-T conditions, suggesting that they are relatively more stable than other species.

Among these generated chemical products, formamide is a crucial precursor molecule that plays a vital role in the synthesis of biomolecules in prebiotic chemistry [24, 25, 35–38]. Thus, we first investigated the formation of formamide. Fig. 3 (a) provides an illustration of the distinct formation pathways of formamide at three P-T conditions. The complete formation processes are shown in Figure S7. At 10 GPa and 1000 K, the formation process began with the dissociation of water molecules, generating OH⁻ and H⁺ ions in the aqueous solution. When the H⁺ ion encountered a CO molecule, a reaction occurred, resulting in the formation of a C-H bond and an aldehyde group (-CHO). Subsequently, the aldehyde group reacted with the NH₃ molecule, leading to the formation of a C-N bond, and ultimately, one N-H bond broke to produce formamide. At 10 GPa and 1400 K, the formation process differs from that at 10 GPa and 1000 K. One N-H bond in NH₃ first broke, leading to the formation of a dissociative amino group (-NH₂). The amino group then reacted directly with a CO molecule, forming the C-N bond. Later, the water molecule dissociated again, providing a hydrogen atom that ultimately contributed to the formation of the formamide molecule. At 13 GPa and 1400 K, the C-N bond was initially formed through the reaction of NH₃ and CO molecules. After a very short time, the dissociated hydrogen atom from the water molecule also bonded to the carbon atoms, forming a C-H bond. Finally, by releasing a hydrogen atom from the NH₃ group, the formamide molecule was generated. Although the formation pathways differ at three P-T conditions, we observed two common features: first, the reactants always include CO, H₂O, and NH₃, and second, the reaction pathways must involve the formation of C-N and C-H bonds and the breakage of N-H bonds.

For the generation of biomolecules in living matter, the formation of C-N bonds is the key step. We further applied the advanced sampling method (see details in method section)

to calculate the free energy profile of the C-N bond formation at three P-T conditions, as shown in Fig. 3(b). The collective variable is the distance between the carbon and nitrogen atoms. At 10 GPa, 1000 K and 13 GPa, 1400 K, the C-N bonds, whose lengths are 1.33 Å and 1.31 Å respectively, are at the metastable states. The free energy decreases upon dissociation of the C-N bond, indicating that breaking C-N bonds at these two P-T conditions are more favorable thermodynamically. The free energy profiles suggest that the energy barriers of the C-N bond dissociation are 17.57 kcal/mol and 16.40 kcal/mol, at 10 GPa, 1000 K and 13 GPa, 1400 K, respectively. As a comparison, at 10 GPa and 1400 K, the free energy increases upon dissociation of the C-N bond (1.31 Å), and the energy barrier is 59.04 kcal/mol, indicating that the C-N bond is thermodynamically and kinetically stable at this P-T condition. The free energy result agrees with the data in Fig 2, where there are more CN-containing species at 10 GPa and 1400 K than at the other two P-T conditions. Additionally, compared with the free energy profile at 10 GPa and 1000 K, there are two more energy minima at the C-N distance of 2.37 Å and 2.45 Å at 10 GPa, 1400 K and 13 GPa, 1400 K, respectively. The free energy increases upon the dissociation of the C-N pair, indicating that these two minima are thermodynamically stable. The C-N distances are larger than that of a typical C-N covalent bond, which strongly implies the presence of an additional atom connecting the two. This is consistent with a wider variety of organic species at these two P-T conditions. Our free energy calculations suggest that the C-N bond formation is favorable at 10 GPa and 1400 K. With increasing the pressure to 13 GPa and keeping the temperature at 1400 K, the carbon and nitrogen atoms tend to be bonded together by a third atom.

After studying the basic chemical products at the three P-T conditions, we now turned to investigate the formation of large biomolecules as potential building blocks of life on Earth. Previous simulations have extensively studied glycine, the smallest amino acid, under various conditions [17, 18, 39]. In our simulations at 10 GPa and 1400 K, we discovered one molecule very similar to glycine, called α -hydroxyglycine. Fig. 4 (a) illustrates the

process of forming α -hydroxyglycine from formamide. The chemical evolution suggests that, a hydrogen atom attacked the formamide molecule, leading to the creation of a protonated formamide molecule, also known as an aminohydroxymethyl radical. Subsequently, a CO_2 molecule reacted with the protonated formamide, resulting in the production of a molecule with the “-N-C-C-” CN-backbone through forming a C-C bond. Finally, another hydrogen atom was captured by a “-COO” group, ultimately yielding the α -hydroxyglycine molecule. In comparison to glycine, α -hydroxyglycine differs by having one H atom and an “-OH” group instead of two H atoms connecting to the α -C. Glycine can be obtained if the “-OH” group is replaced by a single H atom. During this process, the formation of the C-H bond is a crucial step. To identify appropriate P-T conditions for further advancing the chemical evolution of glycine, we calculated the free energy as a function of the C-H distance in Fig. 4 (b). Considering that the CN-backbone of the “ C_2N ” species in the 13 GPa - 1400 K is “-C-N-C-”, very different from the CN-backbone in the glycine molecule, we did not consider this system. From the energy curves, we can see that the energy minima occurs at 1.07 Å for both 10 GPa - 1000 K and 10 GPa - 1400 K, and the energy barriers for C-H breaking are 21.91 kcal/mol and 22.04 kcal/mol, respectively, which are quite similar. However, the change of free energy from C-H bond formation to C-H bond dissociation is more positive at 10 GPa - 1400 K (6.76 kcal/mol) compared with that of 10 GPa - 1000 K (2.63 kcal/mol), which illustrates that 10 GPa - 1400 K condition is still the favorable one for forming C-H bond.

To test if we can also obtain glycine at extreme P-T conditions, we set up a new simulation box containing 5 α -hydroxyglycine, 10 H_2 , and 10 H_2O molecules and perform AIMD simulations at 10 GPa and 1400 K, as shown in Fig. 4(c). Initially, two α -hydroxyglycine molecules would connect to a larger molecule, but later transformed into two new molecules after about 28 ps, dehydroglycine and glyoxylic acid. We mainly focus on dehydroglycine. As the simulation went on, this molecule possessed the amino group when one free proton was bonded to its N atom. After a shorter time, the α -C also captured one proton, resulting

in the final molecular structure of glycine at about 38 ps. Additionally, our observations indicate that once glycine is formed at 10 GPa - 1400 K, it remains at a stable state.

Both proteins and DNA are widely recognized as the important biomolecules for building blocks of life. However, the question of which one came first in the emergence of life remains a topic of debate. This is due to the fact that the replication of DNA relies on the catalytic activity of enzymes, which are a type of protein. Conversely, the production of proteins also needs the guidance of DNA, resulting in a chicken-and-egg dilemma. To solve this problem, a famous hypothesis known as “The RNA world” was proposed, which believed that RNA may occur earlier than DNA and protein [40, 41]. During this stage, the RNA not only have the ability to reproduce themselves and carry genetic information, but also could catalyze certain biological reactions in life activities like enzyme[42, 43]. So the synthesis of RNA plays an important role in the early stage of the origins of life. Generally, RNA is composed of ribose sugar, four kinds of nucleobases, and a phosphate group. Considering that our simulation systems only contain C, H, O, and N elements, we then also explore whether the ribose and nucleobases could be synthesized under extreme conditions.

We first consider Ribose ($C_5H_{10}O_5$), composed solely of C, H, O elements. The formose reaction is a well-known prebiotic pathway for synthesizing ribose from formaldehyde (CH_2O) [44]. Our simulations have generated a few relevant hydrocarbon products (shown in Figures S8 and S9), including formaldehyde molecule (number 1 in Figure S8), so we chose it as the primary reactant of synthesizing ribose. Additionally, to facilitate the synthesis process, the reactants also include a “C₂” molecule, (Z)-ethene-1,2-diol ($C_2H_4O_2$, number 7 in Figure S8). Initially, We constructed a simulation box consisting of 10 (Z)-ethene-1,2-diol molecules and 5 formaldehyde molecules (Figure S10). After about 76 ps, a “C₅” molecule was formed at ~ 10 GPa and 1400 K. However, it could not transform into the structure of ribose after an extended time. We further inserted 5 water molecules to the system, and finally got ribose molecules. The reaction process is shown in Fig. 5 (a), where formaldehyde and “C₂” molecules reacted to form a “C₃” molecule, which subsequently combined with

another “C₂” molecule to form a “C₅” molecule. This “C₅” molecule then evolved into the open-chain form of ribose at about 19 ps.

To analyze the formation process, we calculated the free energy in Fig. 5 (b), where two C-C distances were selected as collective variables labelled as CV1 and CV2. For the first collective variable, two carbon atoms come from formaldehyde and “C₂” molecule, respectively, which are labeled as C1 with yellow color. While for the second collective variable, two carbon atoms are from two different “C₂” molecules, marked as C2 with orange color. Our aim is to determine whether ribose formation follows the C1-C1-C2-C2 connectivity pattern. The free energy landscape shows a clear energy minimum that corresponds to the formation of ribose. However, the C-C distance at this point is larger than the typical C-C bond distance, indicating that the formation of ribose deviates from our initial expectations. To gain further insights, we examined the biased molecular dynamics trajectories and found that the carbon backbone of generated ribose molecule follows the C1-C2-C1-C2 arrangement. By measuring the distances of C1-C1 and C2-C2 in this molecule, we confirm that they correspond to the distances observed at the minimum energy point. Furthermore, an alternative initial configuration for the free energy calculation is also presented in Figure S11. Despite the unexpected bondings of the carbon atoms, the free energy landscape remains a reliable indicator of the ribose formation process, as the region of minimum energy still corresponds to a formation of ribose molecule.

Previous studies showed that the cyclic forms of ribose are abundant in aqueous solutions at room temperature [45]. However, the cyclic forms of ribose were not detected after 90 ps in our simulations (Fig. 5 (a)). We also carried out further simulations to try to generate rings, as illustrated in Figure S12, but there was still no ring formed. However, that does not mean that the cyclic forms of ribose could not be formed under extreme conditions. The simulation time of 90 ps, though relatively long for AIMD simulations, is significantly shorter than the timescales of real chemical evolutions in deep Earth. The spacial limitation under high pressure may restrict the configuration changes of ribose, reducing the probability of the

C4' or C5' hydroxyl group attacking the C1' aldehyde group, which is disadvantageous for producing the furanose form (5-membered ring) or pyranose form (6-membered ring). These two factors suggest that some cyclic formation reactions may be restricted by the shorter timescale and small size of the system in AIMD simulations. To better study the cyclic formation mechanism, we chose the curved open-chain ribose molecules obtained from the previous simulations, as it appears that the C4' or C5' hydroxyl group has a greater chance of reacting with C1' aldehyde group under such narrow space. We built a new simulation box containing three of these ribose molecules and eighteen water molecules. After about 36ps, a furanose form of ribose was formed. Fig. 5 (c) shows the ring formation mechanism, the C4' hydroxyl group first lost a hydrogen atom, leaving a carbonyl group. The oxygen atom then attacked C1' to form the ring, and finally, the carbonyl group on C1' received one dissolved proton in the solution to generate the 5-membered ribose ring. No 6-membered ring was found from our simulations of extreme P-T conditions.

We further applied free energy calculations to study the formation ability of 5- and 6-membered ribose rings at ~ 10 GPa and 1400 K. We chose two C-O distances as the CVs for the two rings, as shown in Fig. 5 (d). The energy minima are at the C-O distance of 1.37 Å for the two ribose forms, indicating the formation of C-O bonds and the rings. Besides, the formation of the C-O bonds lowers the free energy by 11.57 kcal/mol for the 5-membered ribose ring and 5.85 kcal/mol for the 6-membered ribose ring, indicating that the ring formation is thermodynamically more stable and the furanose form of ribose is more favored than the pyranose form at ~ 10 GPa and 1400 K. The free energy result explained why the the pyranose form of ribose is absent in our AIMD simulations. Compared with ambient conditions, high pressure would induce the limited space, which may not support the existence or formation of bigger cyclic form of molecules, so energy barrier for forming 5-membered ring is lower than that of 6-membered ring.

Note that at ambient conditions, the naturally-occurring ribose exists as a mixture of cyclic forms in equilibrium with its open-chain form in aqueous solutions, and the pyranose

form of ribose is the predominant conformation, accounting for approximately 70% [46, 47]. However, despite the thermodynamic stability of the pyranose form of ribose over the furanose form at ambient conditions, the exclusive constituent of the carbohydrate backbone of RNA remains the furanose form of ribose. The reason behind it is still unknown. There are several hypotheses proposed to explain this preference, including silicate(borate)/ribose complexes [48, 49] and temperature gradients [47]. Our finding suggests that extreme P-T conditions in Earth’s upper mantle may also generate the necessary component for assembling RNA molecules. Consequently, it highlights the potential role of upper mantle environment in facilitating the emergence and development of RNA-based life.

We then shifted our attention towards the chemical evolution of nucleobases, which are another essential building blocks of genetic information. There are five naturally-occurring nucleobases: adenine (A), cytosine (C), guanine (G), thymine (T), and uracil (U). Of these, uracil is unique to RNA, so our studies are primarily focused on investigating the formation of uracil molecules under extreme conditions. We first studied the formation of the open-chain “C₄N₂” molecule with the same CN-backbone present in uracil, as illustrated in Fig. 6 (a). Previous experimental studies on the origins of life have suggested that formamide is a crucial molecule for the prebiotic formation of nucleobases, in the presence of mineral or metal oxide catalysts [24], heating[35], and high-energy free radicals [38, 50], so here we also first chose formamide as a reactant. However, after about 144 ps, we did not observe the formation of the “C₄N₂” molecule at 10 GPa and 1400 K, indicating that it is difficult for small molecules to directly synthesize uracil in the AIMD simulations at extreme P-T conditions (Figure S13). Later, we chose the chemical reactants that have closer structural similarities to the “C₄N₂” molecule. The reactant molecules, including “C₄N”, “C₃N₂”, “C₂N₂”, and “C₃”, were generated from our previous AIMD simulations. One previous study suggested that uracil could be synthesized from the reactions between urea and “C₃” molecules [51], so we specifically selected the C₃H₄O₄ molecule (number 10 in Figure S8) and the urea molecule (CH₄N₂O, number 11 in Figure 1) as reactants. The simulation results

are presented in Figure S14. However, regardless of the inclusion of water molecules or the application of different pressure conditions, we do not observe any “C₄N₂” molecules with the CN-backbone of uracil. We conducted eight more AIMD simulations to investigate the possibility of forming uracil through reactions involving those molecules at various pressures and 1400 K (see the Supporting Information).

Particularly, we found that, the C₄H₈N₂O₂ molecule, N-(((λ³-methyl)amino)methyl)-2-hydroxy-2λ³-ethanamide (labeled as “C₄N₂-1”), was formed after about 13 ps in the simulation box consisting of 3 C₃H₈N₂O₂ (number 15 in Fig. 1), 10 H₂O, 10 H₂, and 10 CO molecules, at about 10 GPa and 1400 K. The formation process is provided in Figure S16. Like ribose, the “C₄N₂-1” molecule retained its open-chain form after an extended simulation time of ~ 108 ps.

To study the ring formation of the uracil molecule, we also selected the “C₄N₂-1” molecule with large curvature and built a simulation box containing 6 “C₄N₂-1” and 6 water molecules. Fig. 6 (b) shows that all the “C₄N₂-1” molecules reacted. At 5.6 GPa and 1400 K, linear “C₄N₂-1” molecules became 5-membered and 6-membered rings within a shorter time of about 3.6 ps. Particularly, the elements in the six-membered-ring molecule are the same as those in uracil as shown in Fig. 6(a). At 9.3 GPa and 1400 K, the same 6-membered-ring molecule is also formed. These simulations suggest that it is possible for the open-chain form of molecules with same CN-backbone of uracil to transform into the cyclic form. We further performed free energy calculations to analyze this ring formation reaction. We first chose the distance between the head and tail carbon atoms in the open-chain form of uracil as the CV. The enhanced sampling simulation at ~ 10 GPa and 1400 K produced the same 6-membered-ring molecule as in our previous simulation. Note that the free energy profile suggests that the cyclic form is at the metastable state.

Later we chose allophanic acid (C₂H₄N₂O₃, number 13 in Fig. 1) and (Z)-ethene-1,2-diol (C₂H₄O₂, number 7 in Figure S8) as reactants, and built a new simulation box containing 5 C₂H₄N₂O₃, 5 C₂H₄O₂, and 10 H₂, as shown in Fig.6 (c). At ~ 10 GPa and 1400 K, a “C₅N₂”

molecule, 3-(3-carboxyureido)-2,3-dihydroxypropanoic acid, was formed at around 28.8 ps. This molecule can be considered as the CN-backbone of thymine (T). As the simulation continued, a “C₄N₂” molecule, 2,3-dihydroxy-3-ureidopropanoic acid, labeled as “C₄N₂-2”, was formed. The formation process of these two molecules are shown in Figure S18. We further performed an enhanced sampling simulation to analyze the ring formation process at ~ 10 GPa and 1400 K. The simulation box has one “C₄N₂-2” molecule and 32 water molecules, as shown in Fig. 6 (c). Finally, the molecule with a uracil ring, known as uracil glycol, was successfully synthesized, which is a uracil-like molecule. The free energy curve in Fig. 6 (c) shows that the cyclic form is more stable than the open-chain form, indicating that this uracil-like molecule is possible to form in geological C-H-O-N fluids at extreme P-T conditions. We do not postulate that uracil molecules cannot be synthesized due to the limited time scale and length scale of such atomistic simulations. As molecules containing the uracil ring have already been observed, we are confident that with a longer duration of chemical reactions, it is highly probable to produce complete uracil molecules in geological fluids. The uracil molecule can then serve as a precursor for the synthesis of other three types of nucleobases, providing the necessary components for forming RNA molecules.

CONCLUSIONS

Extensive AIMD simulations have been performed to investigate the chemical reactions of small inorganic molecules under the extreme conditions found in Earth’s upper mantle. Three corresponding P-T systems were considered, i.e., 10 GPa - 1000 K, 10 GPa - 1400 K, and 13 GPa - 1400 K. The simulation results have revealed the potential formation of substantial quantities of organic matter, with the composition and abundance of CN-containing species being profoundly influenced by the specific P-T conditions. Notably, formamide, recognized as a crucial precursor in the production of biomolecules, is observed to readily form under high P-T conditions, and its formation pathways are compared across

different P-T conditions. Furthermore, free energy calculations have confirmed that the 10 GPa - 1400 K condition is particularly favorable for the generation and preservation of CN-containing compounds.

Using the molecules formed, we further explore the formation process of large biomolecules that are directly related to the building blocks of life. Remarkably, glycine, ribose, and uracil-like molecules are successfully synthesized under extreme conditions in our AIMD simulations, thereby providing initial insights into the formation of organic compounds critical to the emergence of life. More importantly, different from that the 6-membered ring of ribose is the majority in solutions at ambient conditions, it is found that formation of 5-membered ring form of ribose is more favorable at Earth’s mantle conditions, which could provide the necessary components for the generation of RNA molecules. Moreover, these compounds have the potential to be transported to the Earth’s surface through geological activities, such as volcanic eruption, consequently contributing to the origins of life. Our comprehensive studies present a novel perspective suggesting that life may have originated from the depths of the Earth’s interior. The findings underscore the profound impact of extreme P-T conditions on the formation of organic matter and provide valuable insights into the mechanisms underlying the emergence of life on our planet.

METHODS

First Principles molecular dynamics simulations (FPMD)

Born-Oppenheimer ab initio molecular dynamics (AIMD) simulations are conducted using the Qbox code[52] to investigate the reactions of C-H-O-N fluids under Earth’s upper mantle conditions. The PBE exchange-correlation functional and ONCV pseudopotentials [53] are utilized, and the Bussi-Donadio-Parrinello (BDP) thermostat, with a relaxation time of 24.2 fs, is employed to control the temperature [54]. To facilitate a larger time step of 0.24

fs, deuterium atoms are used in place of hydrogen atoms in simulations. For the initial setup, the simulation box consists of 15 NH₃, 15 H₂O, 15 H₂, and 15 CO, as depicted in Figure S1. Periodic boundary conditions are applied. Three P-T systems are considered based on Earth's upper mantle conditions: 10 GPa - 1000 K, 10 GPa - 1400 K, and 13 GPa - 1400 K. NPT simulations are carried out initially to achieve the desired system pressure, with the plane-wave energy cutoff set to 85 Ry for the real cell and 70 Ry for the reference cell. The results obtained from NPT simulations are presented in the supporting information (Figure S2). Once the size of the unit cell is converged, a new box will be built based on the equilibrium stage in NPT simulations to run NVT simulations (Table S1). The energy cutoff is adjusted to 65 Ry. Simulations spanning a duration of over 400 ps are conducted under different P-T conditions to ensure the attainment of system equilibrium. All chemical product analyses presented in the main text are obtained from the NVT simulations. Figure S3 shows the total energy and temperature variations during the simulation period. Within the simulation time, the total energy gradually changes little, and the temperature remains stable in all systems. Pressure is also monitored in NVT simulations. To improve computational efficiency, pressure values are not directly imported from NVT simulations but instead calculated by carrying out independent simulations at different time points of NVT simulations with an energy cutoff of 85 Ry. We select random time points under different P-T conditions for the test, which reach approximately 200 ps of NVT simulations, and every data point of pressure is obtained by averaging 12,000 steps, as shown in Figure S4. The total and component values are all within the error ranges. Therefore, we can confidently assert that our NVT simulations are executed under the target P-T conditions.

Free-energy calculations by coupling FPMD simulations with enhanced sampling

To compute the free-energy landscape for compound formation, we employ the adaptive biasing force method (ABF) [55] as implemented in the software package SSAGES [56] coupled with the FPMD software Qbox. Different from other advanced sampling methods that add biases to the energy of the system, this method seeks a flattening of the generalized force. The basic ABF algorithm is shown as follows, the running average of the force in bin k along the reaction coordinate space ξ could be calculated:

$$F_{\xi}(N_{step}, k) = \frac{1}{\nu(N_{step}, k)} \sum_{i=1}^{\nu(N_{step}, k)} F_i(t_i^k)$$
$$F_i(t_i^k) = \frac{d}{dt} \left(M_{\xi} \frac{d\xi}{dt} \right) \Big|_{t_i^k}$$

where $\nu(N_{step}, k)$ is the number of samples collected in bin k after N_{step} steps, $F_i(t_i^k)$ is the i th force sample and t_i^k is the time when force sample i was collected. And the bias force $-\langle \nabla \xi \rangle F_{\xi}(N_{step}, k)$ is added to the system until the landscape is flat in the simulations. It is a “force” method, so it should finally integrate the total biased force for yielding the free energy. For example, the free energy $\Delta A_{a \rightarrow b}$ between two states a and b along the ξ could be calculated by integrating the biasing force:

$$\Delta A_{a \rightarrow b} = - \int_{\xi_a}^{\xi_b} F_{\xi} d\xi \approx - \frac{\xi_b - \xi_a}{k_{\max}} \sum_{k=1}^{k_{\max}} F_{\xi}(N_{step}, k)$$

In free-energy calculations, similar to the FPMD simulations described above, we utilize enhanced sampling simulations in the NVT ensemble, employing the BDP thermostat with a time step of 0.24 fs, using the PBE exchange-correlation functional with plane waves (a 65 Ry energy cutoff), and the ONCV pseudopotential. For each specific calculation, we use different numbers of grids for distance variables to store local estimates of the mean derivative of the free energy surface. Furthermore, we select different kinds of distance between atoms as collective variables (CVs) for different organic compounds.

SUPPORTING INFORMATION

Details of simulations, percentage of the C-N containing species with time, hydrocarbon products and free energy calculation, another strategies of formation of ribose and uracil, and their rings.

ACKNOWLEDGEMENTS

The authors would like to acknowledge support from the Croucher Foundation through the Croucher Innovation Award, Hong Kong Research Grants Council (Projects GRF-16307618, GRF-16306621, and C6021-19EF), National Natural Science Foundation of China (Project 11774072 and Excellent Young Scientists Fund), the Alfred P. Sloan Foundation through the Deep Carbon Observatory, and the Hetao Shenzhen/Hong Kong Innovation and Technology Cooperation (HZQB-KCZYB-2020083).

* dingpan@ust.hk

- [1] Pérez-Villa, A., Pietrucci, F. & Saitta, A. M. Prebiotic chemistry and origins of life research with atomistic computer simulations. *Phys. Life Rev.* **34**, 105–135 (2020).
- [2] Darwin, C. To jd hooker 1 february [1871]. *Darwin Correspondence Project, Cambridge University Library, Cambridge*. <https://www.darwinproject.ac.uk/letter/DCP-LETT-7471.xml> (1871).
- [3] Oparin, A. I. The origin of life on the earth. (1957).
- [4] Miller, S. L. A production of amino acids under possible primitive earth conditions. *Science* **117**, 528–529 (1953).
- [5] Herbst, E. Chemistry in the interstellar medium. *Annu. Rev. Phys. Chem.* **46**, 27–54 (1995).

- [6] Burton, A. S., Stern, J. C., Elsila, J. E., Glavin, D. P. & Dworkin, J. P. Understanding prebiotic chemistry through the analysis of extraterrestrial amino acids and nucleobases in meteorites. *Chem. Soc. Rev.* **41**, 5459–5472 (2012).
- [7] Sleep, N. H. & Zahnle, K. Refugia from asteroid impacts on early mars and the early earth. *J. Geophys. Res.: Planets* **103**, 28529–28544 (1998).
- [8] Takai, K. *et al.* Ultramafics-hydrothermalism-hydrogenesis-hyperslime (ultrah3) linkage: a key insight into early microbial ecosystem in the archean deep-sea hydrothermal systems. *Paleontol. Res.* **10**, 269–282 (2006).
- [9] Miller, S. L. & Bada, J. L. Submarine hot springs and the origin of life. *Nature* **334**, 609–611 (1988).
- [10] Otake, T. *et al.* Stability of amino acids and their oligomerization under high-pressure conditions: implications for prebiotic chemistry. *Astrobiology* **11**, 799–813 (2011).
- [11] Zhang, C. & Duan, Z. A model for c–o–h fluid in the earth’s mantle. *Geochim. Cosmochim. Acta* **73**, 2089–2102 (2009).
- [12] Manning, C. E., Shock, E. L. & Sverjensky, D. A. The chemistry of carbon in aqueous fluids at crustal and upper-mantle conditions: experimental and theoretical constraints. *Rev. Mineral. Geochem.* **75**, 109–148 (2013).
- [13] Sverjensky, D., Daniel, I. & Brovarone, A. V. The changing character of carbon in fluids with pressure: Organic geochemistry of earth’s upper mantle fluids. *Carbon in Earth’s Interior* 259–269 (2020).
- [14] Pan, D. & Galli, G. The fate of carbon dioxide in water-rich fluids under extreme conditions. *Sci. Adv.* **2**, e1601278 (2016).
- [15] Stolte, N. & Pan, D. Large presence of carbonic acid in co₂-rich aqueous fluids under earth’s mantle conditions. *J. Phys. Chem. Lett.* **10**, 5135–5141 (2019).
- [16] Stolte, N., Yu, J., Chen, Z., Sverjensky, D. A. & Pan, D. Water–gas shift reaction produces formate at extreme pressures and temperatures in deep earth fluids. *J. Phys. Chem. Lett.* **12**,

- 4292–4298 (2021).
- [17] Saitta, A. M. & Saija, F. Miller experiments in atomistic computer simulations. *Proc. Natl. Acad. Sci.* **111**, 13768–13773 (2014).
- [18] Goldman, N., Reed, E. J., Fried, L. E., William Kuo, I.-F. & Maiti, A. Synthesis of glycine-containing complexes in impacts of comets on early earth. *Nat. Chem.* **2**, 949–954 (2010).
- [19] Goldman, N. & Tamblyn, I. Prebiotic chemistry within a simple impacting icy mixture. *J. Phys. Chem. A* **117**, 5124–5131 (2013).
- [20] Koziol, L. & Goldman, N. Prebiotic hydrocarbon synthesis in impacting reduced astrophysical icy mixtures. *Astrophys. J.* **803**, 91 (2015).
- [21] Nair, N. N., Schreiner, E. & Marx, D. Glycine at the pyrite-water interface: the role of surface defects. *J. Am. Chem. Soc.* **128**, 13815–13826 (2006).
- [22] Pollet, R., Boehme, C. & Marx, D. Ab initio simulations of desorption and reactivity of glycine at a water-pyrite interface at “iron-sulfur world” prebiotic conditions. *Origins Life Evol. Biospheres* **36**, 363–379 (2006).
- [23] Schreiner, E., Nair, N. N., Wittekindt, C. & Marx, D. Peptide synthesis in aqueous environments: the role of extreme conditions and pyrite mineral surfaces on formation and hydrolysis of peptides. *J. Am. Chem. Soc.* **133**, 8216–8226 (2011).
- [24] Saladino, R., Crestini, C., Pino, S., Costanzo, G. & Di Mauro, E. Formamide and the origin of life. *Phys. Life Rev.* **9**, 84–104 (2012).
- [25] Pietrucci, F. & Saitta, A. M. Formamide reaction network in gas phase and solution via a unified theoretical approach: Toward a reconciliation of different prebiotic scenarios. *Proc. Natl. Acad. Sci.* **112**, 15030–15035 (2015).
- [26] Saladino, R., Botta, G., Pino, S., Costanzo, G. & Di Mauro, E. Genetics first or metabolism first? the formamide clue. *Chem. Soc. Rev.* **41**, 5526–5565 (2012).
- [27] Halfen, D., Ilyushin, V. & Ziurys, L. Formation of peptide bonds in space: a comprehensive study of formamide and acetamide in sgr b2 (n). *Astrophys. J.* **743**, 60 (2011).

- [28] Ligterink, N. *et al.* The formation of the building blocks of peptides on interstellar dust grains. *Proc. Int. Astron. Union* **15**, 216–219 (2019).
- [29] Carballeira, L. & Pérez-Juste, I. Role of the anomeric effect in methanediamines in the gas phase and aqueous solutions. *J. Comput. Chem.* **22**, 135–150 (2001).
- [30] Marks, J. H., Wang, J., Fortenberry, R. C. & Kaiser, R. I. Preparation of methanediamine (CH₂(NH₂)₂)—a precursor to nucleobases in the interstellar medium. *Proc. Natl. Acad. Sci.* **119**, e2217329119 (2022).
- [31] Tossell, J. What happens at the microscopic level when CO₂ reacts with ammonia or amines in solution or on cryogenic surfaces? *Energy Environ. Sci.* **3**, 1079–1091 (2010).
- [32] Belson, D. & Strachan, A. Preparation and properties of isocyanic acid. *Chem. Soc. Rev.* **11**, 41–56 (1982).
- [33] Pranata, J. & Davis, G. D. Computational investigations of reactive intermediates in the acid-catalyzed proton exchange in formamide. *J. Phys. Chem.* **99**, 14340–14346 (1995).
- [34] Sanz, P., MÓ, O., Yáñez, M. & Elguero, J. The effects of C by N replacement on the hydrogen bonding of malonaldehyde: N-formylformimidic acid, N-(hydroxymethyl) formamide and related compounds. *Phys. Chem. Chem. Phys.* **11**, 762–769 (2009).
- [35] Enchev, V. *et al.* Chemical evolution: from formamide to nucleobases and amino acids without the presence of catalyst. *J. Biomol. Struct. Dyn.* **39**, 5563–5578 (2021).
- [36] Saladino, R. *et al.* Meteorite-catalyzed syntheses of nucleosides and of other prebiotic compounds from formamide under proton irradiation. *Proc. Natl. Acad. Sci.* **112**, E2746–E2755 (2015).
- [37] Rios, A. C. Impact synthesis of the RNA bases. *Proc. Natl. Acad. Sci.* **112**, 643–644 (2015).
- [38] Ferus, M. *et al.* High-energy chemistry of formamide: A unified mechanism of nucleobase formation. *Proc. Natl. Acad. Sci.* **112**, 657–662 (2015).
- [39] Wang, L.-P. *et al.* Discovering chemistry with an ab initio nanoreactor. *Nat. Chem.* **6**, 1044–1048 (2014).

- [40] Gilbert, W. Origin of life: The rna world. *nature* **319**, 618–618 (1986).
- [41] Nisbet, E. Origin of life: Rna and hot-water springs. *Nature* **322**, 206–206 (1986).
- [42] McClain, W. H., Guerrier-Takada, C. & Altman, S. Model substrates for an rna enzyme. *Science* **238**, 527–530 (1987).
- [43] Forster, A. C. & Altman, S. External guide sequences for an rna enzyme. *Science* **249**, 783–786 (1990).
- [44] Breslow, R. On the mechanism of the formose reaction. *Tetrahedron Lett.* **1**, 22–26 (1959).
- [45] Drew, K. N., Zajicek, J., Bondo, G., Bose, B. & Serianni, A. S. ¹³C-labeled aldopentoses: detection and quantitation of cyclic and acyclic forms by heteronuclear 1d and 2d nmr spectroscopy. *Carbohydr. Res.* **307**, 199–209 (1998).
- [46] Dewick, P. M. *Essentials of organic chemistry: for students of pharmacy, medicinal chemistry and biological chemistry* (John Wiley & Sons, 2013).
- [47] Dass, A. V. *et al.* Equilibrium and non-equilibrium furanose selection in the ribose isomerisation network. *Nat. Commun.* **12**, 2749 (2021).
- [48] Kolb, V. M. & Zhu, W. Complexes of ribose with silicates, borates, and calcium: Implications to astrobiology. In *Instruments, Methods, and Missions for Astrobiology VIII*, vol. 5555, 70–77 (SPIE, 2004).
- [49] Lambert, J. B., Lu, G., Singer, S. R. & Kolb, V. M. Silicate complexes of sugars in aqueous solution. *J. Am. Chem. Soc.* **126**, 9611–9625 (2004).
- [50] Ferus, M. *et al.* High-energy chemistry of formamide: A simpler way for nucleobase formation. *J. Phys. Chem. A* **118**, 719–736 (2014).
- [51] Choe, J. C. Mechanism of prebiotic uracil synthesis from urea and hc3o+ in space. *Astrobiology* **22**, 1363–1369 (2022).
- [52] Gygi, F. Architecture of qbox: A scalable first-principles molecular dynamics code. *IBM J. Res. Dev.* **52**, 137–144 (2008).

- [53] Hamann, D. Optimized norm-conserving vanderbilt pseudopotentials. *Phys. Rev. B* **88**, 085117 (2013).
- [54] Bussi, G., Donadio, D. & Parrinello, M. Canonical sampling through velocity rescaling. *J. Chem. Phys.* **126**, 014101 (2007).
- [55] Darve, E., Rodríguez-Gómez, D. & Pohorille, A. Adaptive biasing force method for scalar and vector free energy calculations. *J. Chem. Phys.* **128**, 144120 (2008).
- [56] Sidky, H. *et al.* Ssages: software suite for advanced general ensemble simulations. *J. Chem. Phys.* **148**, 044104 (2018).

TABLE I. Classification of CN-containing species and some corresponding molecules.

CN-Containing	Selected molecules
“CN”	CH ₂ NO, CH ₂ NO ₂ , CH ₃ NO, CH ₃ NO ₂ , CH ₄ NO...
“C ₂ N”	C ₂ H ₂ NO ₂ , C ₂ H ₃ NO, C ₂ H ₃ NO ₂ , C ₂ H ₄ NO, C ₂ H ₄ NO ₃ , C ₂ H ₅ NO ₂ , C ₂ H ₅ NO ₃ ...
“CN ₂ ”	CH ₄ N ₂ , CH ₆ N ₂ , CH ₇ N ₂ , CH ₄ N ₂ O...
“C ₂ N ₂ ”	C ₂ H ₂ N ₂ O ₃ , C ₂ H ₃ N ₂ O ₂ , C ₂ H ₃ N ₂ O ₃ , C ₂ H ₄ N ₂ O ₂ , C ₂ H ₄ N ₂ O ₃ , C ₂ H ₅ N ₂ , C ₂ H ₅ N ₂ O, C ₂ H ₅ N ₂ O ₂ , C ₂ H ₆ N ₂ O ₂ , C ₂ H ₇ N ₂ O ₂ ...
“C ₃ N _x ” (“x = 1, 2, 3...”)	C ₃ H ₂ NO ₅ , C ₃ H ₃ NO ₃ , C ₃ H ₄ NO ₃ , C ₃ H ₄ NO ₄ , C ₃ H ₄ NO ₅ , C ₃ H ₆ N ₂ O ₂ , C ₃ H ₇ N ₂ O ₂ , C ₃ H ₈ N ₂ O ₂ ...
“C ₄ N _x ”	C ₄ H ₃ NO ₅ , C ₄ H ₄ NO ₄ , C ₄ H ₄ NO ₅ , C ₄ H ₄ N ₂ O ₄ , C ₄ H ₆ N ₂ O ₃ , C ₄ H ₇ N ₂ O ₄ ...

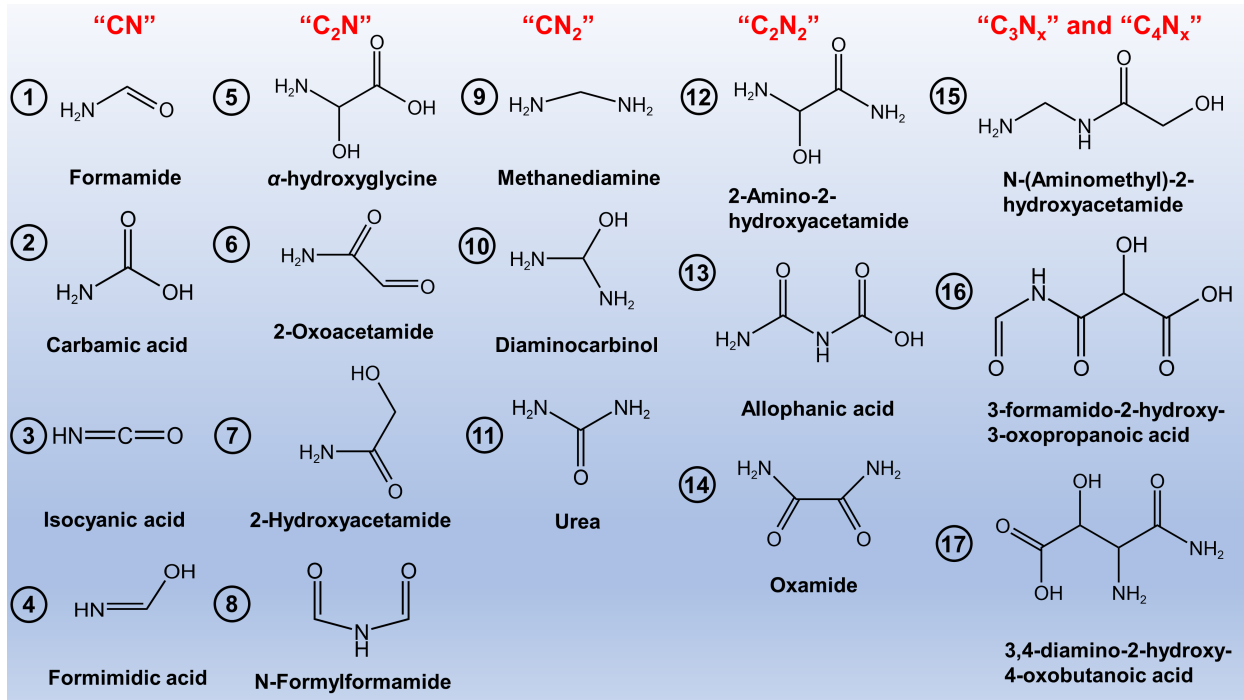


FIG. 1. Chemical structures of the representative products for the “CN”, “C₂N”, “CN₂”, “C₂N₂”, “C₃N_x” and “C₄N_x” species under three different P-T conditions.

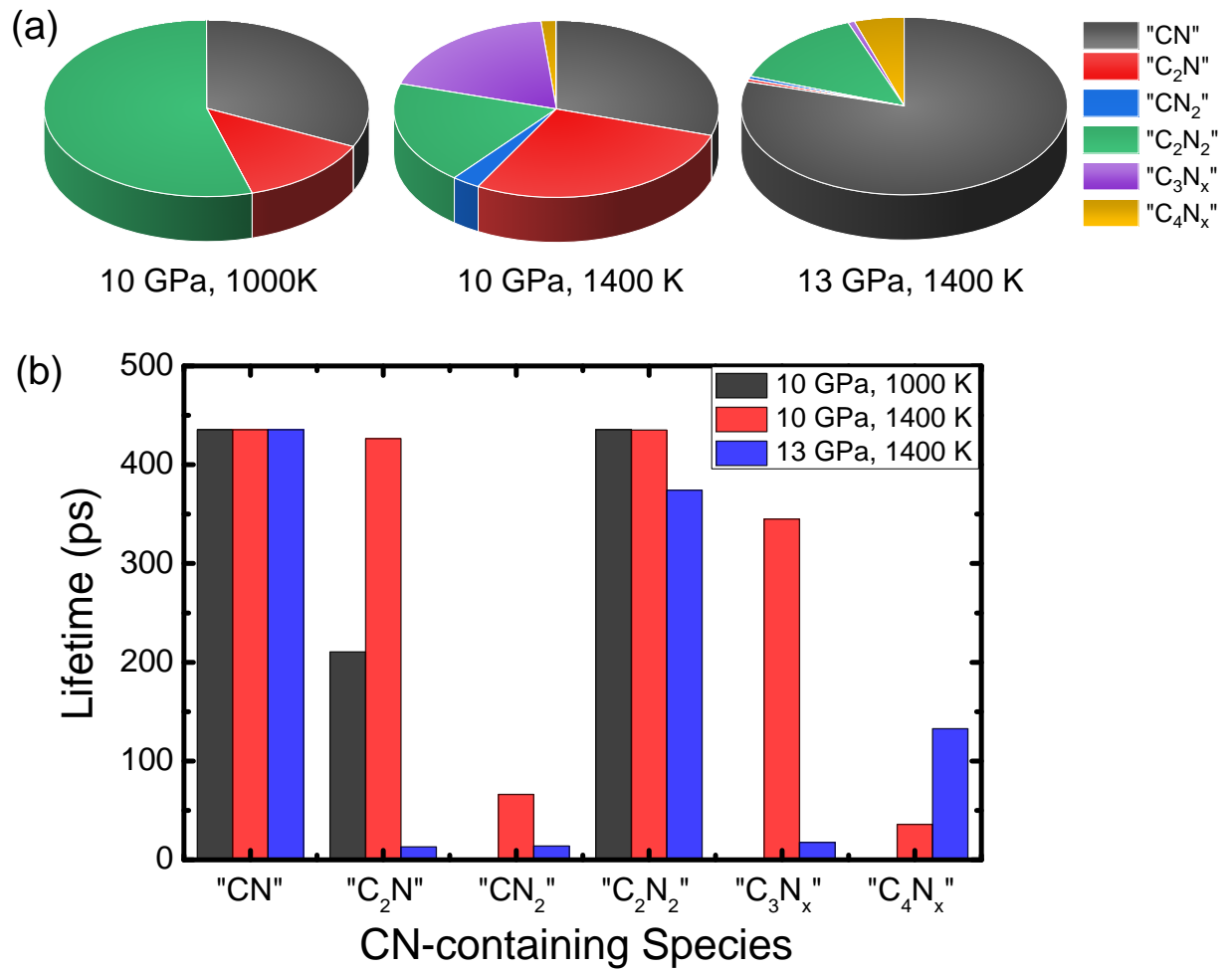


FIG. 2. (a) Total fraction and (b) lifetime of the six kinds of CN-containing species in the NVT simulations for three different P-T conditions.

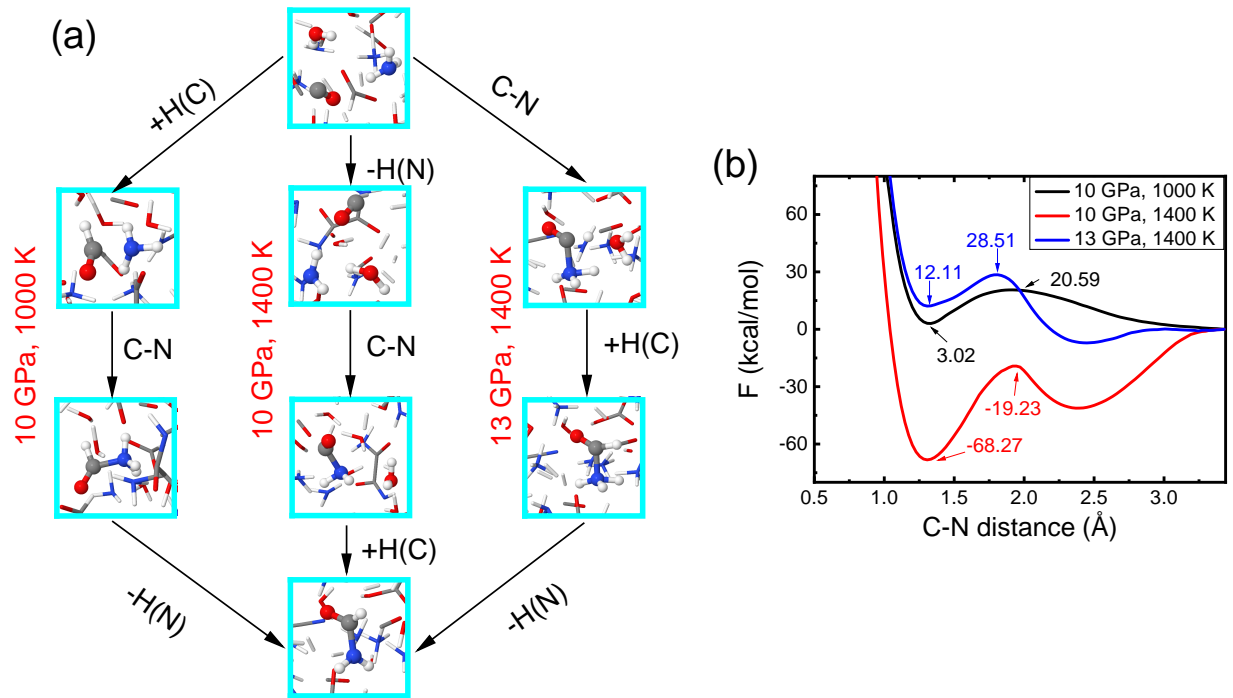


FIG. 3. (a) Formation process of formamide from CO, H₂O and NH₃ in three systems, +H(C), C-N, and -H(N) indicates the formation of a C-H bond, C-N bond, and the breakage of a N-H bond. (b) The free energy curve and C-N distance is selected as the collective variable (CV).

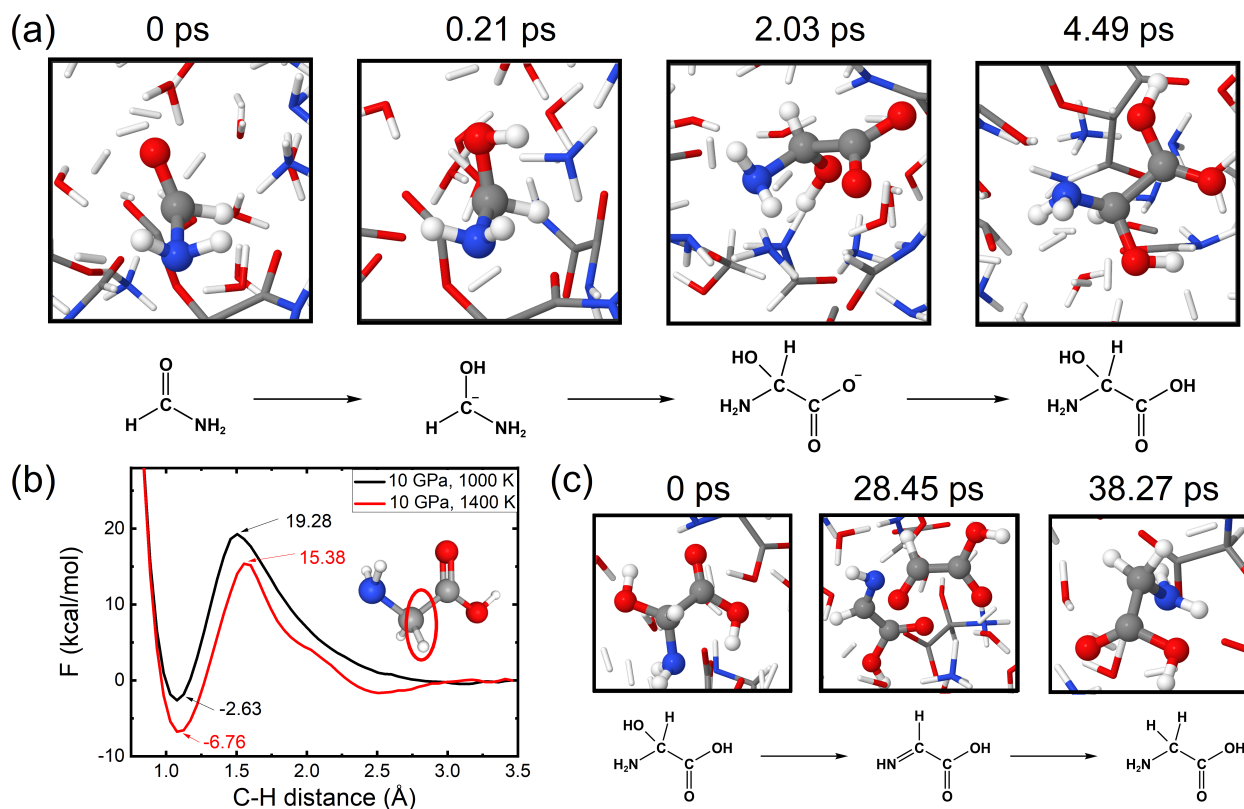


FIG. 4. (a) Formation of α -hydroxyglycine from formamide at 10 GPa - 1400 K. (b) Free energy curve as a function of C-H distance. (c) Formation pathway of the glycine from the 5 α -hydroxyglycine, 10 H_2 , and 10 H_2O at 10 GPa - 1400 K.

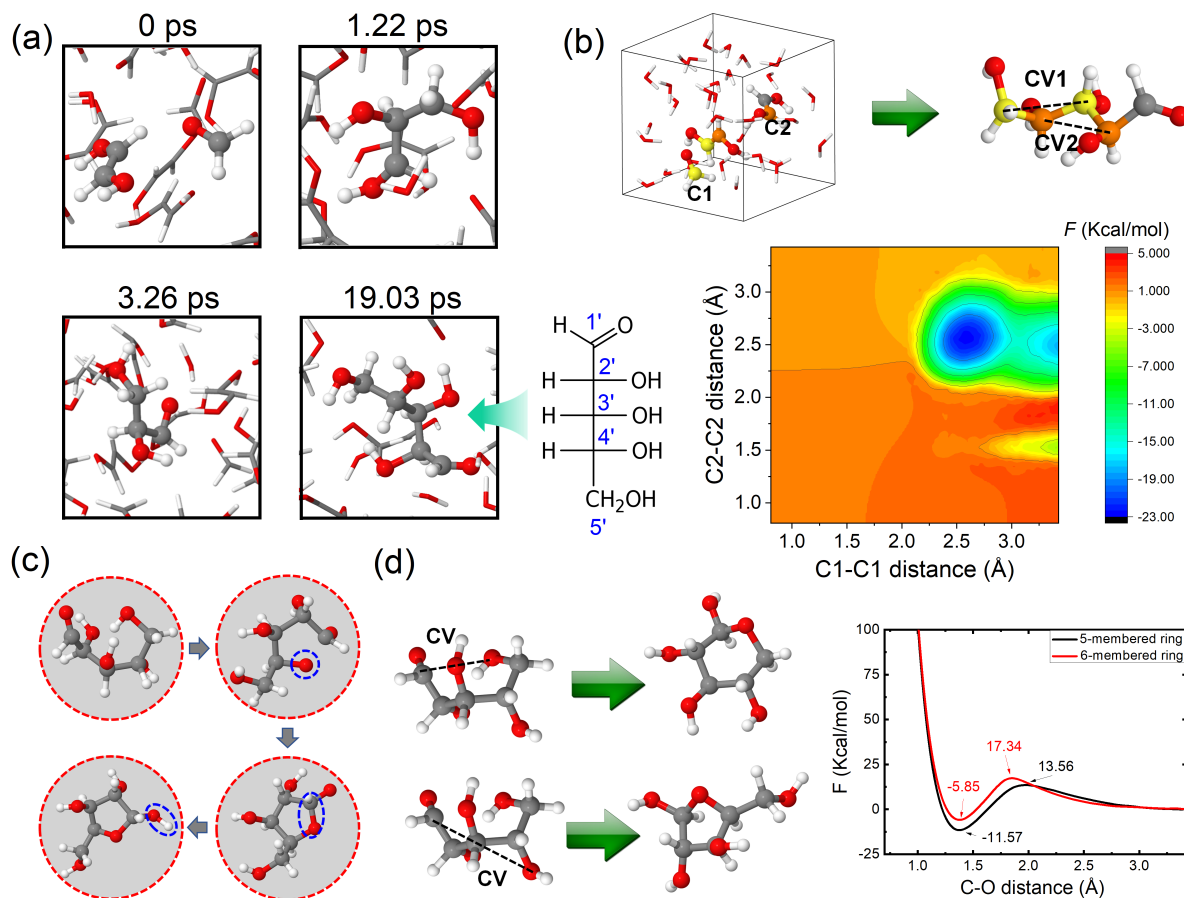


FIG. 5. (a) Formation process of the ribose from 10 (Z)-ethene-1,2-diol, 5 formaldehyde, and 5 water under the condition of 10 GPa - 1400 K. (b) Free energy landscape for analyzing the formation process of ribose, as a function of two kinds of C-C distance as the collective variables. To better distinguish the selected carbon atoms, C1 and C2 are marked by yellow and orange colors, respectively. (c) The evolution process of the ribose from the open chain to a five-membered ring (10 GPa - 1400 K). (d) Comparison of the formation ability of five-membered ring and six-membered ring based on the free energy calculation with the C-O distance as the collective variable.

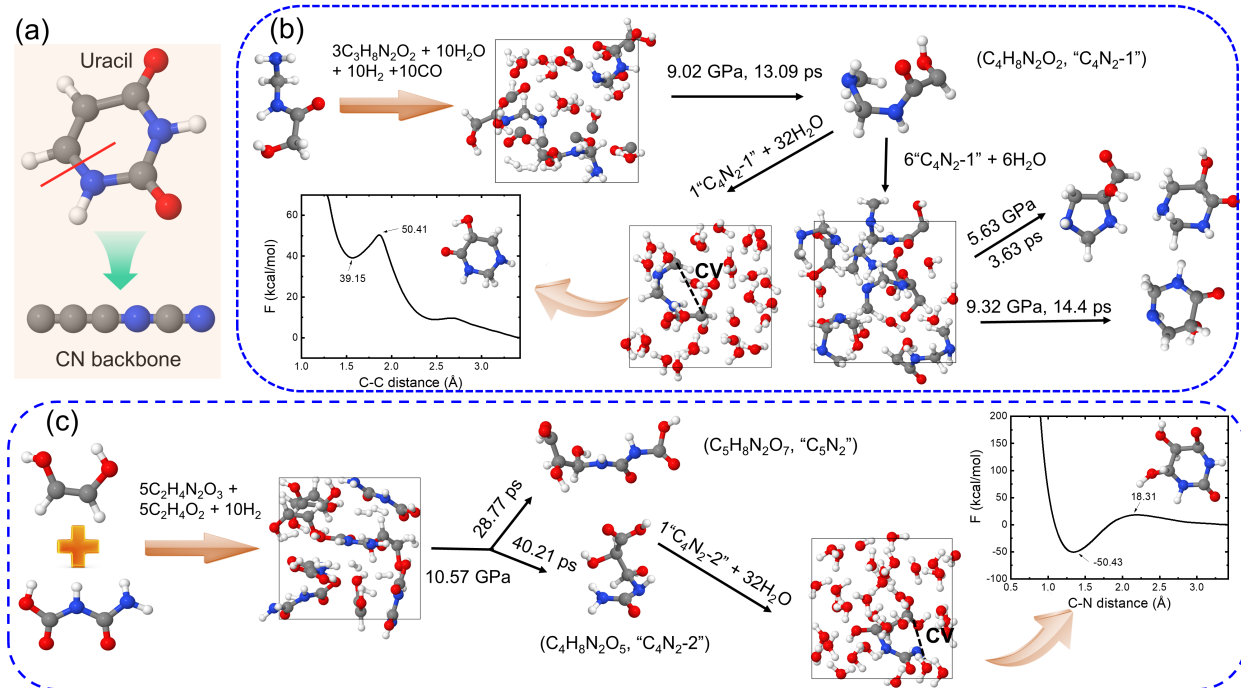


FIG. 6. (a) Structure of the uracil molecule and its open chain form of the CN-backbone when the C-N bond is broken (as denoted in the graph). (b) The formation process of the open chain of the “C₄N₂-1” molecule with CN-backbone of the uracil from the mixture of 3 C₃H₈N₂O₂, 10 H₂O, 10 H₂, and 10 CO, and investigation of uracil ring formation of this molecule by another AIMD simulations (6 “C₄N₂-1” + 6 H₂O) and the free energy calculation (1 “C₄N₂-1” + 32 H₂O), the temperature is kept at 1400 K. (c) Another strategy of the formation process of the open chain of the “C₄N₂-2” molecule with CN-backbone from the mixture of 5 C₂H₄N₂O₃, 5 C₂H₄O₂, and 10 H₂, with the free energy calculation to analyze the uracil ring formation process (1 “C₄N₂-2” + 32 H₂O), the temperature is also 1400 K.